Nonlin. Processes Geophys., 19, 335–343, 2012
www.nonlin-processes-geophys.net/19/335/2012/
doi:10.5194/npg-19-335-2012

Nonlinear Processes in Geophysics

An experimental study of the Atlantic variability on interdecadal timescales

M. Vincze[1], **I. M. Jánosi**[1], **E. Barsy**[1], **T. Tél**[1,2], **and A. Várai**[1]

[1]von Kármán Laboratory for Environmental Flows, Eötvös Loránd University, Pázmány P. s. 1/A, 1117 Budapest, Hungary
[2]Institute for Theoretical Physics and HAS Research Group, Eötvös Loránd University, Pázmány P. s. 1/A, 1117 Budapest, Hungary

Correspondence to: M. Vincze (vincze.m@lecso.elte.hu)

Received: 23 March 2012 – Revised: 18 May 2012 – Accepted: 22 May 2012 – Published: 14 June 2012

Abstract. A series of laboratory experiments has been carried out to model the basic dynamics of the multidecadal variability observed in North Atlantic sea surface temperature (SST) records. According to the minimal numerical sector model introduced by te Raa and Dijkstra (2002), the three key components to excite such a low-frequency variability are rotation, meridional temperature gradient and additive thermal noise in the surface heat forcing. If these components are present, periodic perturbations of the overturning background flow are excited, leading to thermal Rossby mode like propagation of anomalous patches in the SST field. Our tabletop scale setup was built to capture this phenomenon, and to test whether the aforementioned three components are indeed sufficient to generate a low-frequency variability in the system. The results are compared to those of the numerical models, as well as to oceanic SST reanalysis records. To the best of our knowledge, the experiment described here is the very first to investigate the dynamics of the North Atlantic multidecadal variability in a laboratory-scale setup.

1 Introduction

Low-frequency variability has been detected in various sea surface temperature (SST) records in the North Atlantic. Paleoclimatic evidence reaching back to 500 AD (Mann et al., 2009) and instrumental observations since the 1850s suggest that a certain variability in the spectral range of 20–70 yr has been persistently present throughout the centuries and has considerably contributed to the climate variability of the Northern Hemisphere (Sutton and Hodson, 2005).

This phenomenon is widely referred to as Atlantic multidecadal oscillation (AMO), a term coined by Kerr (2000). In the recent years, as paleoclimatic records revealed further information on this signal, the usage of a more appropriate term "Atlantic multidecadal variability" (AMV) started to spread, implying far more complex dynamics than a single oscillatory mode (Vincze and Jánosi, 2011). Numerous studies suggest that at least two dominant timescales can be distinguished within the aforementioned spectral band: one of a 20–30-yr and another of a 50–70-yr variability (Dong and Sutton, 2005; Vellinga and Wu, 2004). Arguments based on field data and numerical results attribute the former to an internal variability of the Atlantic meridional overturning circulation (AMOC), whereas the latter is possibly driven by low-frequency atmospheric forcing and Arctic–Atlantic exchange processes (Frankcombe et al., 2010).

As a measure of this variability, Enfield et al. (2001) introduced an "AMO index" (AMOI), which is defined as the ten-year running mean of detrended SST anomalies, averaged over the North Atlantic (i.e. north of the Equator). In the 1940s, as well as in the past two decades, the Atlantic was relatively warm, corresponding to positive values of AMOI, while for the 1970s the data indicate a rather cold phase (negative AMOI). Note that this variability has a magnitude of 0.2–0.5 °C only; therefore, it is largely suppressed by the signals corresponding to anomalies of shorter (e.g. annual) timescales. Nevertheless, its signature is significantly present in the smoothed SST records.

A certain spatial pattern of the AMV can also be found, associated with the temporal behaviour of AMOI (Kushnir, 1994). Averaging over the warm intervals, one can observe positive SST anomalies all over the North Atlantic basin,

except for the coast of Newfoundland, where a localized negative anomaly is present. During the cold phases, the basin exhibits a similar pattern with the opposite sign: an overall cold anomaly, accompanied with a warm "patch" around Newfoundland.

In order to capture the basic governing dynamics of the AMV, various numerical models were proposed in the past decades, ranging from simple box models (Ou, 2012) to full-up CGCMs (Delworth et al., 2000), which include the effects of, for example, bottom topography or atmospheric coupling. An important member in this hierarchy of models is the idealized ocean-only minimal model, proposed by te Raa and Dijkstra (2002). This setup consists of a rotating rectangular sector of a uniform depth ocean and meridional SST gradient. Frankcombe et al. (2009) showed that a multidecadal oscillatory mode can be excited in this arrangement, by adding temporally and spatially correlated red noise forcing to the SST field, representing ocean–atmosphere interactions. This model is "minimal" in the sense that if any of the three key components (rotation, meridional temperature gradient and thermal noise) is removed, the oscillatory mode can no longer be excited. Note, however, that salinity is not a necessary ingredient of the minimal model, as it does not play an important role in this process.

Based on our previous experience in environment-oriented experiments (Gyüre et al., 2007; Jánosi et al., 2010), we built a laboratory-scale equivalent of the aforementioned minimal model, and carried out measurements to acquire and process the analogues of SST records. Despite the extreme simplicity of our setup, the results were found to be in fairly good agreement with those of the numerical models, and with actual Atlantic SST reanalysis data. To the best of our knowledge, the experiment described here is the very first to investigate the dynamics of the North Atlantic multidecadal variability in a laboratory-scale setup.

The paper is organized as follows: Sects. 2 and 3 discuss the layout of the setup and the basic steps of data processing, respectively. The results are presented in Sect. 4. In Sect. 5 we compare our findings to ocean SST reanalysis records, applying the data evaluation methods used for the experimental data processing.

2 The experimental setup

Our experiment has been carried out in a rectangular acrylic tank, divided into three sectors by two internal vertical walls, as depicted in Fig. 1. The central domain of length $L = 68$ cm and width $D = 25$ cm was filled up to height $H = 10$ cm with tap water. One of the side sectors – separated by a copper internal wall from the central domain – was packed full of melting ice, enough to keep the temperature in this separated compartment at (0 ± 0.1) °C for up to 5 h (the average duration of our experimental runs). On the opposing vertical sidewall, an electric heating element was mounted, capable

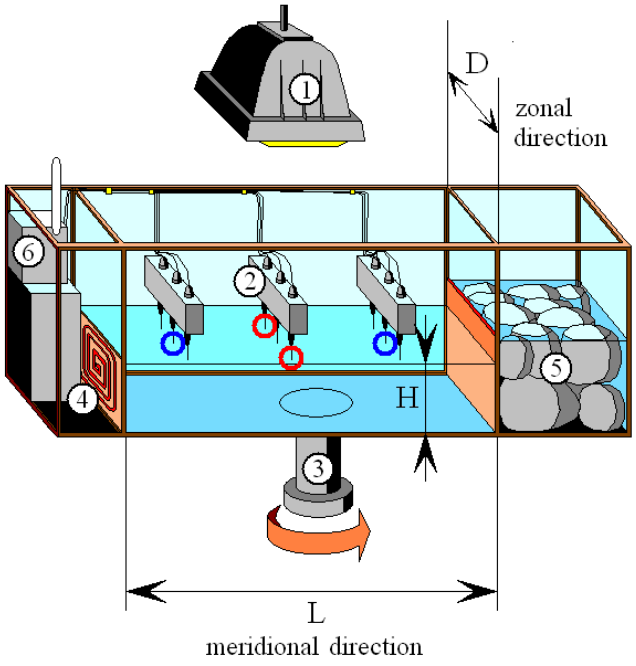

Fig. 1. Schematic drawing of the setup. 1: lamp (for the surface heat flux perturbation), 2: digital temperature sensors (nine in total), 3: axis of rotation (the direction of rotation is also indicated), 4: electric heating module ("Equator"), 5: the cooling sector packed full of ice ("polar region"), 6: radio transmitter for real time data acquisition. The geometric parameters L, D and H are indicated, together with the corresponding terminology ("zonal" and "meridional"), used throughout the paper. The thermometer pairs, from which the "meridional" and "zonal" temperature difference anomaly records were obtained, are marked by blue and red circles, respectively.

of releasing a maximum flux of $0.3\,\mathrm{W\,cm^{-2}}$. These two heat sources provided the analogue of the meridional temperature gradient in our setup.

The differential heating at the sidewalls led to the formation of a full-depth single-cell overturning background flow that is visible in the dye patterns shown in the snapshots of Fig. 2. Note that, for a "sideways convection" arrangement, there does not exist a critical Rayleigh number, which implies that *any* temperature difference ΔT between the sidewalls can initiate such an overturning flow. The typical values of the basin crossing time of the overturning ranged between 300 and 1000 s, depending on ΔT. Naturally, a larger "meridional" temperature difference initiates faster overturning, which is of great importance in setting the timescale of the observed variability, as discussed later.

The tank was mounted onto a platform, rotating at period $P = (3.0 \pm 0.05)$ s. Nine digital thermometers, placed into the uppermost 1 cm of the working fluid, were arranged uniformly to measure the temperature in the central domain of the tank. The frequency of temperature recording was set to $1\,\mathrm{s^{-1}}$.

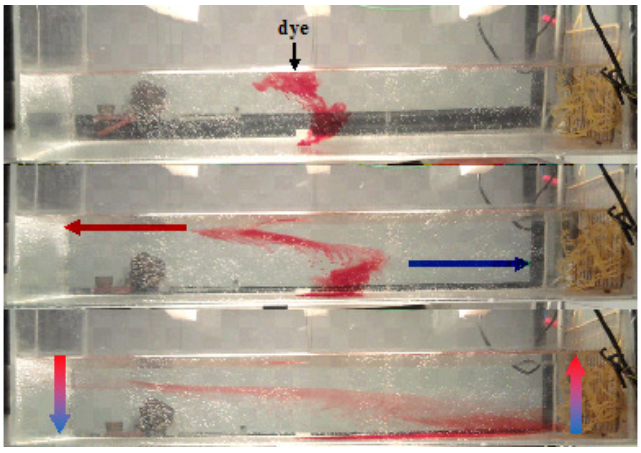

Fig. 2. Three subsequent snapshots of the background flow in a non-rotating control experiment, visualized by red dye injected in the middle of the tank. The full-depth overturning circulation is clearly visible. The arrows indicate the direction of the cold bottom flow (blue) and the warm surface flow (red).

Besides temperature gradient and rotation, the third key component in the minimal models of multidecadal variability is the presence of a spatially correlated and temporally red noise-like surface heat flux perturbation (representing annual variability and the interactions between the sea surface and the atmosphere). This effect was modelled by a halogen lamp, mounted 50 cm above the water surface (not co-rotating). The lamp radiated markedly in the infrared spectral range; thus, it was able to generate spatially quasi-homogeneous temperature anomalies on the order of 0.5 °C all over the water surface (whereas the values of ΔT varied between 0.25 and 1.75 °C). The lamp was switched on and off according to a stochastic sequence, controlled by a computer. In this algorithm the time intervals between the subsequent switches (either on or off) were drawn randomly from a Gaussian distribution of mean $m = 200$ s and standard deviation $\sigma = 50$ s. This set the timescale of the external heat flux perturbation to approximately 400 s, or 130 P. This timescale corresponds to a seasonal-annual variability in the forcing. However, besides its direct effect on the surface temperature, lamp heating also leads to turbulent convective "atmospheric" dynamics in the closed air box above the water surface in the tank, which mimics daily, atmosphere-driven variability, or "weather".

In a test run where only the lamp forcing was active (i.e. neither differential sidewall heating, nor rotation was present), the characteristic response time or "restoring timescale" of the surface temperatures was found to be $\tau \sim 100$ s (33 P). This value was obtained by fitting exponential saturation curves to the temperature response signals recorded during a sequence of lamp switches.

3 Data processing

We intended to observe the laboratory-scale analogue of the dynamics described by te Raa and Dijkstra (2002) and Frankcombe et al. (2009). In those minimal models, the dominant timescale is set by the time that it takes for a patch-like sea surface temperature anomaly to cross the basin in the zonal direction. To find a similar crossing time in our experimental setup, one first needs to calculate the characteristic horizontal velocity U in a rotating, thermally driven flow. In such an arrangement (see, e.g. Jánosi et al. (2010)), U can be estimated as

$$U \approx \frac{\alpha g \Delta T H}{2\Omega L} = 1.4 \times 10^{-4} \mathrm{m\,s^{-1}}, \quad (1)$$

where $\alpha = 4.3 \times 10^{-4}\,^{\circ}\mathrm{C}^{-1}$ is the volumetric thermal expansion coefficient of freshwater, g is the gravitational acceleration, $\Delta T \approx 1\,^{\circ}$C denotes the characteristic "meridional" temperature difference between the two ends of the basin (on distance L), and $\Omega = 2.094\,\mathrm{s^{-1}}$ represents the angular velocity of the tank, corresponding to period P, and $H = 10$ cm is the aforementioned water height in the setup. From here, the time of crossing the tank width D can be estimated as $D/U \approx 1700$ s, or approximately 570 P. Note that in this reasoning U was estimated from the *meridional* temperature difference; yet, we intended to calculate the characteristic timescale of a *zonal* crossing. This can be justified by the argument that the flow in our setup can be treated as quasi-geostrophic, where the zonal and meridional components of the flow velocity are generally on the same order of magnitude. Such estimations and the preliminary inspection of the obtained temperature records yielded the selection of the range 1500–5000 s (500–1667 P) for further analysis. Melting of the water ice in the cooling compartment of the tank also imposed an important constraint on the length of the quasi-stationary part of the experimental runs, and thus on the upper limit of the selected spectral band. Hence, we were unable to resolve variability on timescales longer than $\sim$2000 P significantly. Future experiments involving electric cooling are intended to explore this regime of the dynamics that might correspond to the long-period AMV mode (50–70 yr), mentioned in the Introduction.

Although for the real ocean the multidecadal mode is usually quantified in terms of basin-scale averages of local temperature anomalies (Enfield et al., 2001), it can also be detected directly from the differences of pointwise SST records at large distances from each other (see Sect. 5). Analogously, in order to eliminate the signals from external sources (most notably, our spatially correlated "lamp noise", but also the tiny daily temperature changes in the laboratory), we chose to analyze the temperature differences between the digital thermometers.

After the start of a given experimental run, the system needed approximately one hour (1200 P) time to reach a quasi-stationary state. The records of this transient phase

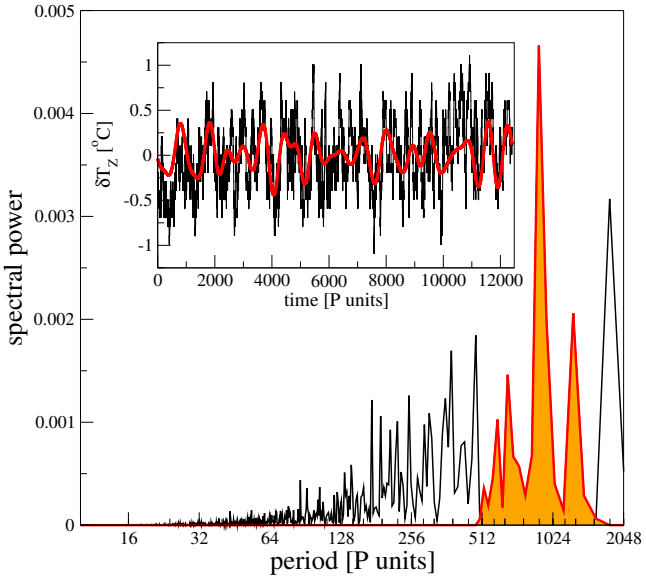

Fig. 3. A typical "zonal" temperature difference (δT_Z) signal before and after band-pass filtering (inset), and the corresponding spectral band in an experimental run where "lamp noise" is present. The time unit was taken to be the revolution period P. Note the log scale in the horizontal axis of the spectrum.

were dropped, and subsequent steps of data processing were carried out only for the remaining part of the time series. We applied band-pass filtering, retaining the aforementioned range of interest (periods between 500 and 1667 P). A typical "zonal" temperature difference signal, δT_Z, before and after filtering, and the corresponding spectra are plotted in Fig. 3.

4 Results

For an ocean-scale numerical minimal model, it has been found that the presence of the meridional temperature gradient and rotation are necessary but not sufficient conditions to initiate a marked multidecadal oscillation, once a realistic parametrization of surface heat boundary conditions is applied (Frankcombe et al., 2009). However, it has also been shown that by adding a spatially correlated noise term to the surface heat forcing, this otherwise damped eigenmode still becomes excited.

A similar amplification mechanism was demonstrated in our setup by a series of control experiments. In Fig. 4 the filtered signal and the corresponding power spectrum of Fig. 3 are repeated, together with those of two control runs. In the first test (red curve), only the "lamp noise" was present (neither rotation, nor side heating/cooling). The other control run (orange curve) was conducted in the opposite arrangement, i.e. with rotation and differential side heating, but without "lamp noise". It is clearly visible that the largest amplitudes

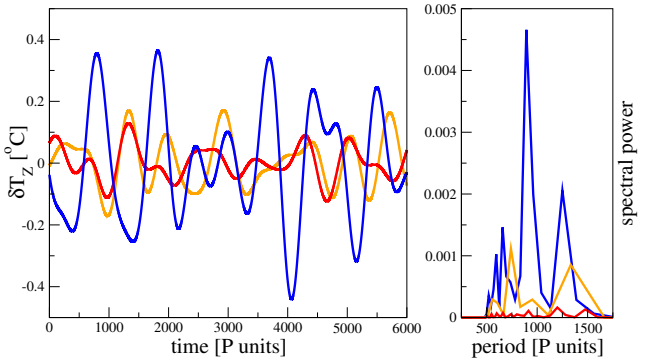

Fig. 4. Comparison of the filtered "zonal" temperature difference anomaly (δT_Z) time series (left panel) and their power spectra (right panel) for three runs: "lamp noise" only (red), side heating and rotation, but no lamp (orange), and an all-up case (blue).

can be observed in the case when all three components were present. Note that the introduction of "lamp noise" forcing yielded significant amplification in the spectral range of our interest (i.e. 500–1667 P), although the characteristic timescales associated with this "lamp noise" are an order of magnitude smaller. The principle of "noisy" forcing is similar to the case of Frankcombe et al. (2009); yet, the fact that the penetration depth of infrared radiation into water cannot be scaled down to a laboratory tank leads to differences in the mechanism of perturbation. In contrast to the ocean, in our setup even the bottom of the basin experiences detectable warming if the lamp forcing is turned on. During the "off" phases, the water surface cools first, while a significant amount of the heat originating from the preceding "on" phase is still stored deeper in the basin. This surface cooling decreases static stability near the top boundary, creating descending plumes, which cause small perturbations in the overturning background flow. This perturbation is present if the amplitude of lamp noise in the surface temperature variability is on the order of $\sim$0.5 °C, which is comparable to the aforementioned typical values of ΔT. This is also different in the numerical model, where the characteristic amplitude of SST noise is an order of magnitude smaller than ΔT.

Next, using the average "meridional" temperature difference $\langle \Delta T_M \rangle$ as a control parameter, we evaluated the periods corresponding to the largest spectral amplitude for seven experimental runs at different values of side heating. $\langle \Delta T_M \rangle$ was obtained directly by averaging over the measured "meridional" surface temperature differences throughout the given run, obtained from the records of the two thermometers, which are marked by blue circles in Fig. 1. The periods were acquired from the "zonal" temperature difference anomalies (δT_Z), measured by the thermometers with red circles in Fig. 1. From Eq. (1) one can conclude that the patch crossing time, and hence the period of the oscillatory mode, scales with ΔT^{-1}. This assumption fairly agrees with our finding that a clearly decreasing trend can be observed,

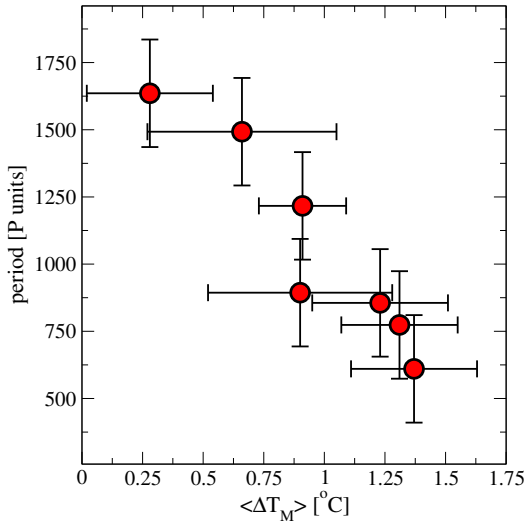

Fig. 5. Period of the largest observed Fourier component of the band-pass filtered zonal temperature difference anomalies (δT_Z), as a function of the average meridional temperature difference.

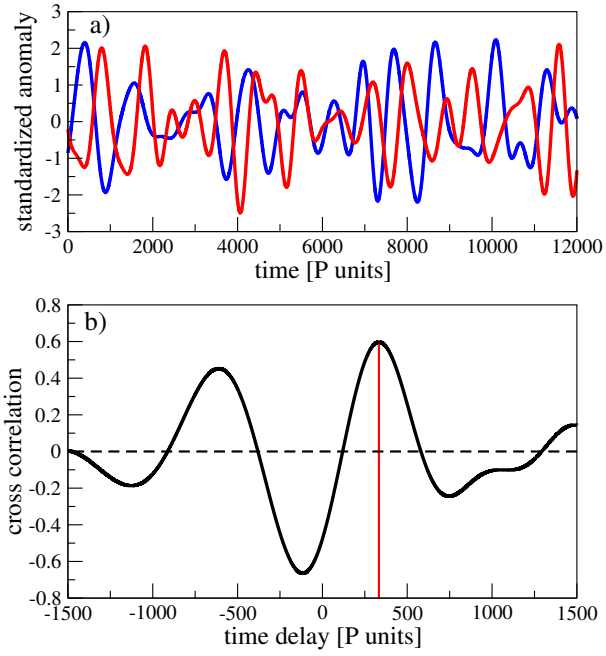

Fig. 6. (a): band-pass filtered, standardized signals of the "meridional" δT_M (blue) and the "zonal" δT_Z (red) temperature difference anomalies. Note the phase shift. **(b)**: cross-correlation diagram of the above two time series, exhibiting a maximum at 333 P.

as visible in Fig. 5. A similar dependence on Equator-to-Pole temperature difference has already been reported in the aforementioned numerical minimal model (Dijkstra, 2006). However, the divergence of the oscillation period for even smaller values of ΔT could not be resolved in this experiment, as under such conditions the period would already have been larger than the upper limit of the selected spectral band of our interest, which was determined by the maximum measurement length.

As a "mechanistic indicator" associated with the *spatial pattern* of the multidecadal variability, Dijkstra et al. (2006) proposed to measure the phase lag between east-west and north-south temperature differences. Inspired by this idea, we processed the "meridional" and "zonal" temperature difference anomaly signals (δT_M and δT_Z) accordingly. It is worth mentioning that Dijkstra et al. (2006) obtained these differences using zonally and meridionally *averaged* temperature signals in their study, instead of pure differences of a pair of pointwise temperature records. This definitely yielded a more robust indicator of the dynamics; however, in the case of our setup such averaging would have introduced a significant bias. Looking at the arrangement of the nine thermometers in our tank (see Fig. 1), it is easy to notice that with averaging over the "latitudes" and "longitudes" of such a 3×3 array of sensors, the signals at the corners would be taken into account twice, both in the zonal and in the meridional averages. We also note here that, in order to obtain δT_M, the signal of the "northern" thermometer was subtracted from that of the "southern" (S–N), and for δT_Z the "eastern" signal was subtracted from the "western" (W–E). Two such detrended, standardized and band filtered records are presented in Fig. 6a. In order to quantify the phase shift between the two time series, cross correlation analysis was conducted with a maximal lag of 5000 s (1667 P). The correlation diagram for this particular run is depicted in Fig. 6b. We chose the location of the first maximum at a positive lag as a measure of the phase shift, which was found to be at 1000 s (333 P) in this case, corresponding to a cross correlation value of about 0.6. Interestingly, in this case δT_M seems to lead δT_Z, contrary to the findings of te Raa and Dijkstra (2002). The reason for this disagreement needs to be clarified in future experiments, involving high resolution detection of the surface temperature patterns by a co-rotating infrared camera. The differences in the geometry of the basin and in the method of surface heat forcing might be responsible for this deviation from numerical results.

To reveal the true spatio-temporal pattern of the zonal propagation, the filtered temperature anomaly time series $\delta T(t)$ of three individual thermometers at the same "meridional" coordinates were combined into Hovmöller diagrams. Cubic splines were used to interpolate the temperature field between the measurement locations. A slice of such a diagram is shown in Fig. 7, for the same experiment as the one of Fig. 6. It is visible that the zonal displacement of an anomaly is predominantly "westward", i.e. it tends to move towards the left of the horizontal range. Similar patterns have been obtained earlier using a GCM (Frankcombe et al., 2010). However, eastward propagating anomalies are also present in the diagram, implying more complex dynamics than in the original (noise-free) model of te Raa and Dijkstra (2002), in

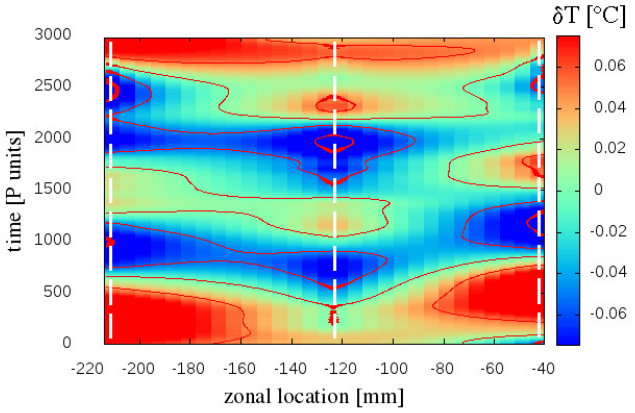

Fig. 7. Hovmöller diagram of a "zonal" slice of band-pass filtered temperature anomalies in our setup. The "meridional" location of the three thermometers (on which the diagram is based on) was 15 cm from the heating side of the tank (i.e. at ∼0.2 L distance). The zonal positions of the three thermometers are marked by vertical dashed lines. The rest of the temperature field was interpolated by cubic splines. Note the similarities to the Hovmöller plots in Frankcombe et al. (2010), obtained from GCM runs.

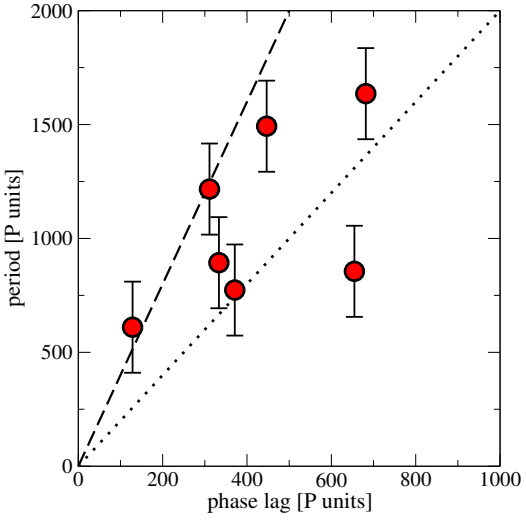

Fig. 8. Period of the largest observed Fourier component of the band-pass filtered zonal temperature difference anomalies (δT_Z) as a function of the phase lag between the meridional and zonal temperature difference anomalies (obtained via cross correlation analysis). The dotted line represents $y = 2x$; the dashed line marks $y = 4x$. The fact that most of the data points lie between the two lines implies positive correlation.

which a pure westward propagation was found. This issue hopefully will be settled by conducting technically more advanced future experiments using an infrared camera to obtain more accurate Hovmöller plots than the one of Fig. 7, which is based on data from three thermometers only.

Theoretically, the mechanism of multidecadal oscillation is based on the principle of quasi-geostrophic *thermal wind balance*, which enables a meridional temperature anomaly to initiate an anomalous zonal velocity perturbation. In return, this anomalous overturning pushes the patch towards a meridional sidewall, which leads to a zonal temperature gradient, and hence, to the excitation of a meridional overturning anomaly (te Raa and Dijkstra, 2002). This interplay between temperature and velocity anomalies drives the observed pattern formation in the system and sets the timescale of the oscillation. As a consequence of this reasoning, one would expect a correlation between the above discussed zonal-meridional phase lags and the period of the oscillation itself. Figure 8 shows this dependence for seven experimental runs. For each run, the phase lag value was obtained via the aforementioned cross-correlation method.

This relation is not nearly as clear as the $\langle \Delta T_M \rangle$ dependence of Fig. 5; yet, a certain trend is present: in the vast majority of the measurements, the observed phase lags are found to be between quarter and half a period (see dotted and dashed lines in Fig. 8), implying correlation. Naturally, for a clear oscillatory mode with one single frequency and one persistent, permanently cycling surface patch (a "thermal Rossby wave"), the phase lag between zonal and meridional temperature differences would be exactly one fourth of a period. However, for a "lamp noise"-induced dynamics present here, it is not surprising at all that the spatial and temporal behaviour appears to be more complex.

5 Discussion

For a better comparison of our findings with the phenomena in the North Atlantic, we carried out a similar analysis on actual SST data, obtained from the NOAA Kaplan Extended SST V2 data set (Kaplan et al., 1998). This reanalysis data set stores monthly averaged SST anomaly values from 1856 to present, with a global coverage of resolution $5 \times 5°$.

To imitate our measurement technique, we selected four grid points in the four "quarters" of the North Atlantic basin: The northern location (N) lies in the vicinity of Iceland (62.5° N, 22.5° W); the southern (S) around Cape Verde, off the coast of Mauritania (12.5° N, 22.5° W); the western site (W) was selected in the region of Newfoundland (47.5° N, 57.5° W); and the eastern location (E) was picked at the Celtic Sea, nearby the British Isles (47.5° N, 7.5° W).

Firstly – as in the case of experimental data processing – we acquired the period corresponding to the largest amplitude on the interdecadal timescales, and determined the appropriate spectral range for the subsequent band-pass filtering, using the W–E signal (Fig. 9). The maximal peak was found at a period of 7580 days (or approximately 20.8 yr), which led to the selection of the range between 5000 and 12 500 days (or 13.7–34.2 yr).

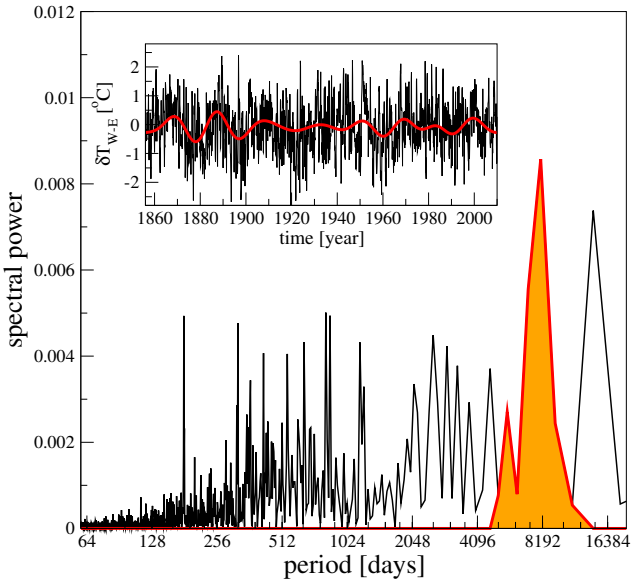

Fig. 9. Monthly averaged zonal temperature difference anomaly signal (inset) and its power spectrum, as measured between the region of Newfoundland and the British Isles. The band-pass filtering retained the periods between 167–411 months, or 5000–12 500 days.

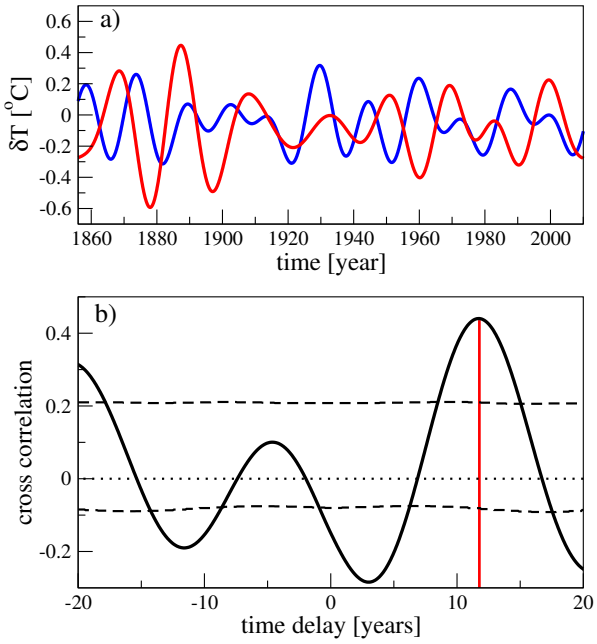

Fig. 10. (a): band-pass filtered signals of the meridional S–N (blue) and the zonal W–E (red) temperature difference anomalies. **(b)**: cross-correlation diagram of the above two time series (the dashed lines represent the 95 % confidence interval).

Next, we determined the characteristic phase shift between the filtered W–E and S–N records, the analogues of δT_{Z} and δT_{M} in the experimental setup. These time series and their cross correlation diagram are presented in Fig. 10. The first maximum at a positive lag was found at around 4200 days (or 12 yr) with a correlation value of 0.45. These data appear to agree with other, much more detailed reanalysis results (see, e.g. (Sinha and Topliss, 2006), where eastward propagating SST anomalies have been identified with characteristic basin crossing times of ~ 10 yr). As mentioned before, both the minimal numerical model of te Raa and Dijkstra (2002) and our results imply that the SST anomalies *predominantly* tend to propagate westward (though, some counterexamples were found in our setup, as discussed in the previous section). In reality, wind-driven surface currents (most notably, the Gulf Stream in the case of the North Atlantic, as reported by Sinha and Topliss, 2006) definitely affect the circulation of such anomalies. Nevertheless, what is of importance here is the order of magnitude agreement between the observed basin crossing timescale of an SST patch and the lag between meridional and zonal temperature differences.

Obviously, our laboratory setup is vastly different from the actual North Atlantic; nevertheless, we carried out an order of magnitude estimation to see whether the experimental results of Fig. 5 are consistent with those obtained from the field data. For this purpose a scale transformation was applied. The period P of a revolution around the rotational axis (i.e. a day in the case of Earth) provided an appropriate natural timescale. The temperature difference parameter ΔT is taken to be the value of $\langle \Delta T_{\mathrm{M}} \rangle$ (or $\langle \Delta T_{\mathrm{S-N}} \rangle$ in the case of the ocean), and can be expressed in terms of the non-dimensional thermal Rossby number Ro_{T} (see, e.g. (Jánosi et al., 2010)), which has the form of

$$Ro_{\mathrm{T}} = \frac{\alpha g \Delta T H}{4\Omega^2 R^2}, \tag{2}$$

where R denotes a characteristic horizontal length scale of the system. As for the laboratory setup, we used $R = D$, and all the other geometric and material parameters had the same values as in Sect. 3. For the North Atlantic, we set $R = 6.4 \times 10^6$ m, the radius of Earth (also coincides with the maximum width of the Atlantic basin) as length scale, $\alpha = 3.0 \times 10^{-4}\,^{\circ}\mathrm{C}^{-1}$, as the volumetric thermal expansion coefficient of seawater, $\Delta T = \langle \Delta T_{\mathrm{S-N}} \rangle = 15\,^{\circ}\mathrm{C}$, the average Equator-to-Pole SST difference and $\Omega = 7.272 \times 10^{-5}\,\mathrm{s}^{-1}$, the angular velocity of Earth. The proper setting of the height scale H of the multidecadal variability is not trivial, as this would require knowledge about the vertical structure of the velocity fields associated with this variability, on which only sparse field data exist. As for now, the penetration depth of the multidecadal anomaly is still a matter of debate. Subsurface signatures of this oscillation have already been detected down to a depth of 400 m using expendable bathythermograph (XBT) data (Frankcombe et al., 2008), but according to the best of our knowledge, no such analyses have been carried out so far for deeper regions. As an order of magnitude estimate, we used $H = 1000$ m. This set of parameters yielded $Ro_{\mathrm{T}} \approx 0.5 \times 10^{-4}$ for the North Atlantic, whereas for

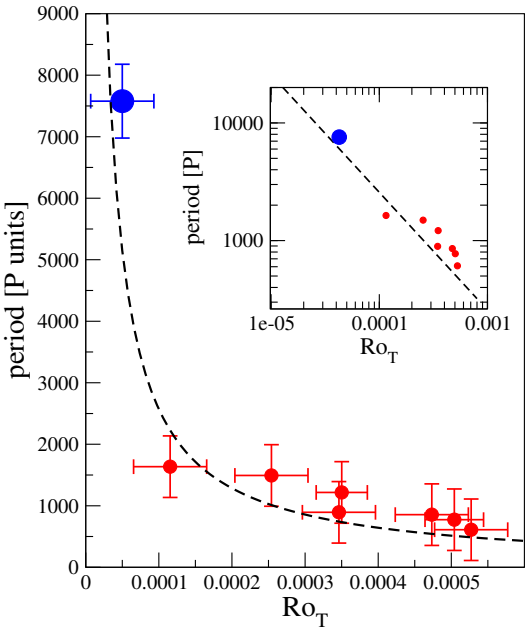

Fig. 11. Non-dimensional period values (in P or day units) versus the non-dimensional temperature (thermal Rossby number Ro_T) obtained from the laboratory experiments (red) and from the ocean reanalysis data (blue). The dashed line represents a $y = ax^{-1}$ dependence. The same values are presented on log-log scale in the inset.

the laboratory setup its values were found to be in the range of $Ro_T \approx (1;5) \times 10^{-4}$.

The non-dimensional experimental data points (red) of the period, together with the value obtained from the field data (blue), are shown in Fig. 11. The dashed line denotes a fit of $f(x) = a/x$ to the *experimental* data (based on the argument in Sect. 4 that the period is inversely proportional to the temperature gradient). Interestingly, the oceanic data point also appears fairly close to the fitted curve, which suggests that the processes in this setup might indeed be driven by similar dynamics to that present in the actual ocean. We emphasize, however, that the almost perfect match of the oceanic data point to the fit might be misleading. Obviously, the North Atlantic is far from a rectangular basin, and the selection of the appropriate geometric parameters for this case is not trivial at all, as mentioned above. What is of importance here is the orders of magnitude agreement between the natural phenomena and those observed in our laboratory setup.

In this experimental work, we studied the laboratory-scale equivalent of a simplified minimal model of the North Atlantic multidecadal variability. The sensitivity of the system to noise-like external heat perturbations and to the meridional temperature gradient – which were predicted by earlier numerical works (Dijkstra, 2006; Frankcombe et al., 2009) – has been confirmed. Signatures of a propagating surface pattern corresponding to this oscillation mode have also been observed. Moreover, the results were found to be in fairly good agreement with field data. However, even within this minimal model, there are still many parameters (e.g. the geometric dimensions of the tank) that could be adjusted in future experiments, to test whether the above proposed nondimensionalization is indeed sufficient to link the oceanic phenomena to the ones observed in the laboratory.

Acknowledgements. The inspiring and highly useful discussions with H. A. Dijkstra are acknowledged. This work was supported by the Hungarian Science Foundation under Grant no. OTKA NK72037 and NK100296. The project is also supported by the European Union and is co-financed by the European Social Fund (grant agreement no. TAMOP 4.2.1./B-09/KMR-2010-0003).

Edited by: R. Grimshaw
Reviewed by: two anonymous referees

References

Delworth, T. L. and Greatbatch, R.: Multidecadal Thermohaline Circulation Variability Driven by Atmospheric Surface Flux Forcing, J. Climate, 13, 1481–1495, doi:10.1175/1520-0442(2000)013¡1481:MTCVDB¿2.0.CO;2, 2000.

Dijkstra, H. A.: On the interaction of SST modes in the North Atlantic Ocean, J. Phys. Oceanogr., 36, 286–299, 2006.

Dijkstra, H. A., te Raa, L.A., Schmeits, M. and Gerrits, J.: On the physics of the Atlantic Multidecadal Oscillation, Ocean Dynam., 56, 36–50, 2006.

Dong, B. and Sutton, R. T.: Mechanism of interdecadal thermohaline circulation variability in a coupled ocean-atmosphere GCM, J. Climate, 18, 1117–1135, 2005.

Enfield, D. B., Mestas-Nunez, A. M., and Trimble, P. J.: The Atlantic Multidecadal Oscillation and its relation to rainfall and river flows in the continental US, Geophys. Res. Lett., 28, 2077–2080, doi:10.1029/2000GL012745, 2001.

Frankcombe, L. M., Dijkstra, H. A., and von der Heydt, A.: Subsurface signatures of the Atlantic Multidecadal Oscillation, Geophys. Res. Lett., 35, L19602, doi:10.1029/2008GL034989, 2008.

Frankcombe, L. M., Dijkstra, H. A., and von der Heydt, A.: Noise-induced multidecadal variability in the North Atlantic: excitation of normal modes, J. Phys. Oceanogr., 39, 220–233, doi:10.1175/2008JPO3951.1, 2009.

Frankcombe, L. M., von der Heydt, A., and Dijkstra, H. A.: North Atlantic Multidecadal Variability: An investigation of dominant time scales and processes, J. Climate, 23, 3626–3638, 2010.

Gyüre, B., Bartos, I., and Jánosi, I. M.: Nonlinear statistics of daily temperature fluctuations reproduced in a laboratory experiment, Phys. Rev. E, 76, 037301, doi:10.1103/PhysRevE.76.037301, 2007.

Jánosi, I. M., Kiss, P., Homonnai, V., Pattantyús-Ábrahám, M., Gyüre, B., and Tél, T.: Dynamics of passive tracers in the atmosphere: laboratory experiments and numerical tests with reanalysis wind fields, Phys. Rev. E, 82, 046308, doi:10.1103/PhysRevE.82.046308, 2010.

Kaplan, A., Cane, M., Kushnir, Y., Clement, A., lumenthal, M., and Rajagopalan, B.: Analyses of global sea surface temperature 1856–1991, J. Geophys. Res., 103, 18567–18589, 1998.

Kerr, R. A.: A North Atlantic Climate Pacemaker for the Centuries, Science, 288, 1984–1985, doi:10.1126/science.288.5473.1984, 2000.

Kushnir, Y.: Interdecadal Variations in North-Atlantic Sea-Surface Temperature and Associated Atmospheric Conditions, J. Climate, 7, 141–157, 1994.

Mann, M. E., Zhang, Z., Rutherford, S., Bradley, R. S., Hughes, M. K., Shindell, D., Ammann, C., Faluvegi, G., and Ni, F.: Global Signatures and Dynamical Origins of the Little Ice Age and Medieval Climate Anomaly, Science, 326, 1256–1260, doi:10.1126/science.1177303, 2009.

Ou, H.: A minimal model of the Atlantic Multidecadal Variability: its genesis and predictability, Clim. Dynam., 38, 775–794, doi:10.1007/s00382-011-1007-3, 2012.

Sinha, B. and Topliss, B.: A description of interdecadal time-scale propagating North Atlantic sea surface temperature anomalies and their effect on winter European climate, 1948–2002, J. Climate, 19, 1067–1079, doi:10.1175/JCLI3646.1, 2006.

Sutton, R. T. and Hodson, D. L. R.: Atlantic Ocean forcing of north American and European summer climate, Science, 309, 115–118, 2005.

te Raa, L. A. and Dijkstra, H. A.: Instability of the thermohaline circulation on interdecadal time scales, J. Phys. Oceanogr., 32, 138–160, 2002.

Vellinga, M. and Wu, P.: Low-latitude freshwater influence on centennial variability of the Atlantic thermohaline circulation, J. Climate, 17, 4498–4511, 2004.

Vincze, M. and Jánosi, I. M.: Is the Atlantic Multidecadal Oscillation (AMO) a statistical phantom?, Nonlin. Processes Geophys., 18, 469–475, doi:10.5194/npg-18-469-2011, 2011.